Assembling Exfoliated Layered Double Hydroxide (LDH) Nanosheet/Carbon Nanotube (CNT) Hybrids via Electrostatic Force and Fabricating Nylon Nanocomposites

Shu Huang,[†] Hongdan Peng,[†] Weng Weei Tjiu,[‡] Zhe Yang,[†] Hong Zhu,[†] Tao Tang,[§] and Tianxi Liu*[,†,§]

Key Laboratory of Molecular Engineering of Polymers of Ministry of Education, Department of Macromolecular Science, Fudan University, Shanghai 200433, P. R. China, Institute of Materials Research and Engineering, ASTAR (Agency for Science, Technology and Research), 3 Research Link, Singapore 117602, and State Key Laboratory of Polymer Physics and Chemistry, Changchun Institute of Applied Chemistry, Chinese Academy of Sciences, Changchun 130022, P. R. China

Received: September 13, 2010; Revised Manuscript Received: November 8, 2010

In this paper, Co−Al layered double hydroxide (LDH) and carbon nanotubes (CNT) have been assembled to form exfoliated LDH nanosheet/carbon nanotube hybrids via electrostatic force. The assembling process and nanostructures of exfoliated LDH/CNT hybrids were investigated by zeta potential, Raman spectroscopy, transmission electron microscopy (TEM), and X-ray diffraction (XRD). The assembly mechanism of LDH with CNT was also discussed. Furthermore, the unique three-dimensional (3D) hybrids thus prepared were used as reinforcing nanofillers to enhance the performance of polyamide 6 (PA6). It was found that the synergic effect of the CNT and LDH nanoplatelets resulted in homogeneous dispersion of the hybrid nanofillers throughout the PA6 matrix and strong combination with the matrix, thus providing an efficient mechanical improvement for the PA6 nanocomposites.

1. Introduction

Layered double hydroxides (LDH), a family of layered inorganic compounds consisting of stacks of positively charged metal hydroxide layers with anions in the interlayer, have been widely studied in fields of catalysts,[1−3] storage and triggered release of functional anions,[4−8] optical materials,[9−11] flame retardants,[12−14] and nanofillers.[15,16] However, many of the applications are largely restricted because microsized LDH usually stacks together to form a layered structure with a thickness of tens of nanometers. In order to maximize the utility of LDH, the most effective solution to this problem may be delamination of LDH into single layers.[17,18] Single-layered LDH usually has high aspect ratios of about 1000 or more, because exfoliated LDH has a diameter of about several millimeters and thickness of about 1 nm. Recently, Sasaki et al. successfully delaminated various LDHs to single-layered nanosheets by using the microsized hexagonal LDH as precursor and formamide as a delaminating reagent.[19−21]

Compared with two-dimensional (2D) LDH, carbon nanotubes (CNT) are one kind of one-dimensional (1D) nanomaterials which are commonly used as nanoscale fillers for fabrication of polymer nanocomposites due to their outstanding mechanical, electrical, and chemical properties.[22−25] However, the applications of both LDH and CNT are greatly limited by their intrinsic properties, such as easily forming bundles or layered stacks when the surface is not modified.[26,27] The introduction of CNTs into the interlayer of LDH sheets impedes restoring the LDH structure. By acting as a "spacer", the CNTs increase the interlayer distance between the LDH nanosheets by dozens of nanometers.[28] As a result, the CNT spacers ensure that a high specific surface area and other unique properties exhibited by exfoliated 2D LDHs are retained in its dry state. Therefore, the hybridization of 1D nanotubes and 2D lamellar flakes leads to three-dimensional (3D) hybrid nanomaterials which are very promising and crucial as it can enable versatile and tailormade properties with excellent performances far beyond those of the individual materials. For instance, the combined 3D clay−CNT polymer nanocomposites show extraordinary mechanical and energy-absorbing properties.[29,30] Therefore, it is very necessary to prepare CNT/LDH hybrids which are anticipated to have promising applications in polymer reinforcement, electrochemical energy production and storage, and sensors.

Recently, several groups described the in situ growth of CNTs on various LDHs and formed 3D hierarchical nanocomposites.[31−34] However, there are several disadvantages about growing CNTs on the surfaces of LDHs. First, after calcination, the hydrotalcite-like structure of the LDHs was lost, leaving metal oxides and spinellites as the major elements. Second, the growth of CNTs on the surfaces of LDH platelets cannot effectively exfoliate the LDH stacks to single-layered nanosheets. Third, the LDH used for growing CNTs was limited to those LDHs containing transition metals, which are often used as the catalyst for growing CNTs.

In this work, we report a simple method for preparing exfoliated LDH/CNT hybrids through mixing positively charged LDHs and negatively charged CNTs. It was found that the colloidal suspension of LDHs was broken down, and both LDHs and CNTs coparticipated in the formamide after introducing CNTs. This behavior assures the strong interaction between LDH nanosheets and CNTs. We proposed a model to describe the coassembling process of positively charged LDH nanosheets with negatively charged CNTs via electrostatic force. Furthermore, the homogeneously exfoliated LDH/CNT hybrids thus

* To whom correspondence should be addressed. Phone: +86-21-55664197. Fax: +86-21-65640293. E-mail: txliu@fudan.edu.cn.
[†] Fundan University.
[‡] Agency for Science, Technology and Research.
[§] Chinese Academy of Sciences.

10.1021/jp1087256
Published on Web 12/02/2010

obtained were used to prepare high-performance polyamide 6 nanocomposites.

2. Experimental Section

2.1. Reagents and Materials. Pristine multiwalled carbon nanotubes (denoted as p-CNT; length, 10−30 μm; diameter, < 10 nm; purity, 95%), produced by the chemical vapor deposition (CVD) method, were supplied by the Chengdu Institute of Organic Chemistry, Chinese Academy of Sciences, China. All other reagents were purchased from Sinopharm Chemical Reagent Co. Ltd. and used as received. Ultrapure Milli-Q water was used throughout all experiments.

2.2. Synthesis of Co−Al−NO_3 LDHs and Modification of CNTs. Co−Al−NO_3 LDHs used in this study were synthesized on the basis of our previous report.[35] First, Co−Al−CO_3 LDH sample was synthesized using the hydrolysis method under hydrothermal condition. A typical preparation process was described as follows: $CoCl_2 \cdot 6H_2O$, $AlCl_3 \cdot 6H_2O$, and urea were dissolved in 100 mL of deionized water to give final concentrations of 10, 5, and 35 mM, respectively. The aqueous mixture was allowed to react in a 100 mL Teflon-lined autoclave at 100 °C for 24 h. After cooling to room temperature, the solid products were filtered, subsequently washed with deionized water and anhydrous ethanol several times, and finally air dried at room temperature. The as-prepared Co−Al−CO_3 LDH was then treated with a NaCl−HCl mixed solution (1 M NaCl and 3.3 mM HCl in 1 L deionized water) for 12 h to complete the decarbonation of LDH and thus obtained the Co−Al−Cl LDH. The Co−Al−NO_3 LDH was prepared by treating the Cl^- intercalated LDH with a conventional anion-exchange process. Typically, 0.5 g of the NaCl−HCl-treated LDH sample was dispersed into 500 cm^3 of an aqueous solution containing 0.1 M $NaNO_3$. The subsequent procedures were the same as those described above.

Negatively charged CNTs (i.e., CNT−COONa) were prepared according to the modified Salzmann's method.[35,36] Typically, p-CNTs were ultrasonicated for 30 min and then refluxed in 9 M HNO_3 in a round-bottom glass flask at 100 °C for 12 h. After cooling to room temperature, they were vacuum filtered through a 0.22 μm Millipore PTFE membrane, washed with deionized water until a neutral pH of the filtrate was reached, and then dried at 50 °C overnight. Then, the obtained oxidized CNTs were stirred in 4 M NaOH solution under nitrogen at 80 °C for 8 h. The products (denoted as CNT−COONa) were filtered and washed by distilled water thoroughly until a neutral pH of the filtrate was reached and then dried at 50 °C overnight.

2.3. Fabrication of LDH Nanosheet/Carbon Nanotube Hybrids. CNT and LDH solutions with a concentration of 1 mg/mL were prepared by adding 200 mg of CNT−COONa and Co−Al−NO_3 LDH into 200 mL of formamide, respectively; after stirring for 1 h, the LDHs and CNTs were quickly dispersed in formamide and colloidal suspensions were obtained. The LDH/CNT hybrid materials were prepared by mixing 200 mL of CNT solution with 200 mL of LDH solution in a flask, which was tightly sealed after purging with nitrogen gas. The mixture was vigorously shaken by a mechanical shaker at a speed of 160 rpm for 2 days. After sedimentation for 72 h, the LDH/CNT hybrids were precipitated and then filtered, washed by distilled water thoroughly, and then dried at 50 °C overnight.

2.4. Preparation of Polyamide 6/LDH/CNT Hybrid Nanocomposites. Polyamide 6 (PA6)/(LDH/CNT) hybrid (ternary) nanocomposites were synthesized on the basis of our previous report.[38] A desired amount of LDH/CNT hybrids and 40 g of ε-caprolactam were taken in a three-necked round-bottom flask. The mixture was sonicated at 80 °C for 60 min, and then 4 g of 6-aminocaproic acid was added to the suspension. The flask was transferred to a preheated oil bath (250 °C) and heated for 6 h with mechanical stirring under a nitrogen atmosphere. The products (ternary PA6/hybrid nanocomposites) were mechanically crushed and soaked in boiling water for 1 h to extract the unreacted monomers and oligomers and then dried at 90 °C under vacuum for 24 h for subsequent use. For comparison, binary PA6/LDH and PA6/CNT nanocomposites were synthesized under the same experimental conditions.

2.5. Characterization. Transmission electron microscopy (TEM) images were recorded on a Philips CM300 FEG TEM instrument operated under an acceleration voltage of 300 kV. A scanning electron microscope (SEM, Tescan 5136 MM) was used to observe the morphology of LDH samples. The SEM samples were coated with gold prior to observation. X-ray diffraction (XRD) patterns of the samples were conducted on an X'Pro X-ray diffractometer with Cu Kα radiation (λ = 0.1548 nm) under a voltage of 40 kV and a current of 40 mA. FTIR spectra were recorded with a 4 cm^{-1} spectral resolution on a Nicolet Nexus 470 spectrometer equipped with a DTGS detector by signal averaging 64 scans. IR samples were in the form of KBr pellets containing 2 wt % predried samples. Zeta-potential measurements were conducted on a Malvern Zetasizer NanoZS system with irradiation from a 632.8 nm He−Ne laser. The samples were filled in folded capillary cells and measured using a mixed mode method combining fast field reversal and slow field reversal, which eliminated electroosmotic effects. Raman spectra were measured on a Dilor Labram-1B Raman spectrometer using a He−Ne laser at 632.8 nm as the light source. The tensile tests were carried out using an Instron universal material testing system (Mode 5567) at room temperature with a gauge length of 25 mm and crosshead speed of 5 mm/min. Film samples (with a thickness of 1 mm) were prepared by compression molding in a press at a temperature at 250 °C for 10 min, followed by quickly quenching in an ice/water bath. The quenched films were finally punched into dog-bone specimens with dimensions of 63.5 × 9.53 × 3.18 mm^3 (Die ASTM D-638 Type V) using a CEAST hollow die punch (mode 6051). At least six specimens were tested for neat PA6 and its nanocomposites.

3. Results and Discussion

Figure 1a shows the TEM image of highly crystalline and monodispersive Co−Al−CO_3 LDH sample. As can be seen, the sample typically consists of uniform and thin hexagonal platelets with a mean lateral size as large as 5 μm. The interlayer CO_3^{2-} must be converted to NO_3^- because NO_3^- LDHs were found to have the best swelling delamination behavior. An effective method based on decarbonation and anion exchange was used to exchange the interlayer CO_3^{2-} into NO_3^-.[20] After salt−acid treatment, as shown in XRD patterns (Figure 2), the basal reflections with *d*-spacing values of 0.75 and 0.375 nm (corresponding to 003 and 006 reflections, respectively) for the CO_3^{2-} form completely disappeared, and thereby new series of intense basal reflections at lower 2θ angles appeared instead, suggesting that decarbonation was successful. Owing to incorporation or intercalation of Cl^-, the basal spacing of the LDHs is increased from 0.75 to 0.78 nm for the 003 reflection. When being further exchanged by NO_3^-, the interlayer space of the 003 reflection is increased to 0.89 nm. The FTIR spectra (Figure 3) of Co−Al−NO_3 LDHs also provide evidence about the presence of NO_3^- (absorption band at 1384 cm^{-1}). A broad absorption band in a wavenumber range of 3000−3700 cm^{-1}

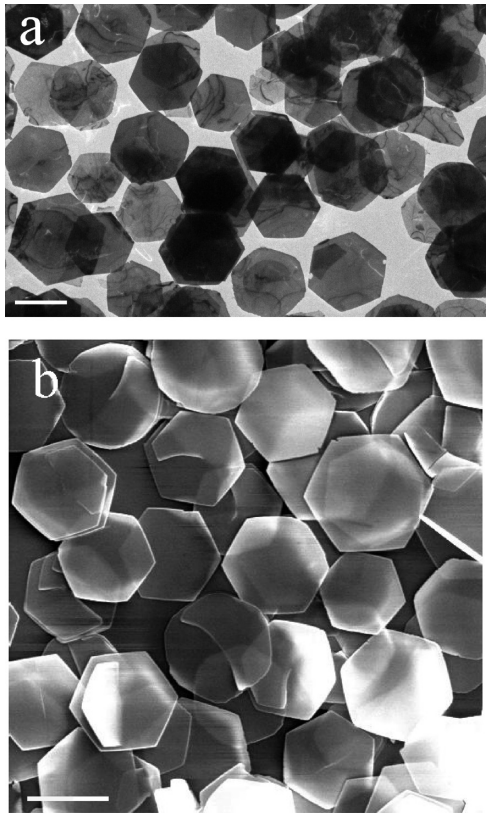

Figure 1. TEM image of (a) Co−Al−CO_3 LDH, and SEM image of (b) Co−Al−NO_3 LDH. The scale bars correspond to 5 μm.

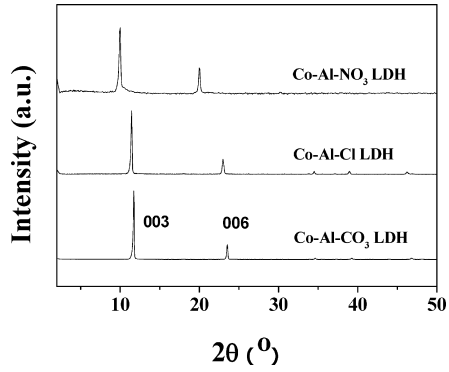

Figure 2. XRD patterns of (a) CO_3^{2-}, (b) Cl^-, and (c) NO_3^- LDH samples.

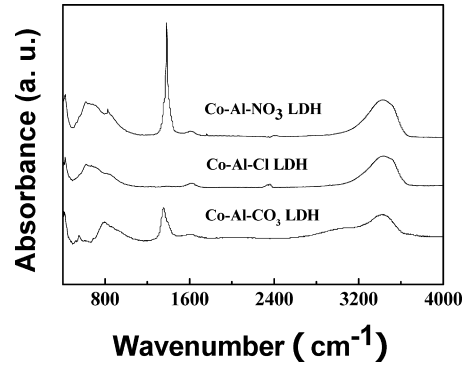

Figure 3. FTIR spectra of (a) CO_3^{2-}, (b) Cl^-, and (c) NO_3^- LDH samples.

and absorption around 1630 cm^{-1} are attributed to stretching and bending modes of water existing in the interlayer, respectively.[20,35] The SEM image (Figure 1b) shows that the obtained Co−Al−NO_3 LDH sample exhibits almost the same morphology and size as the CO_3^{2-} LDH sample, suggesting that no acid corrosion takes place.

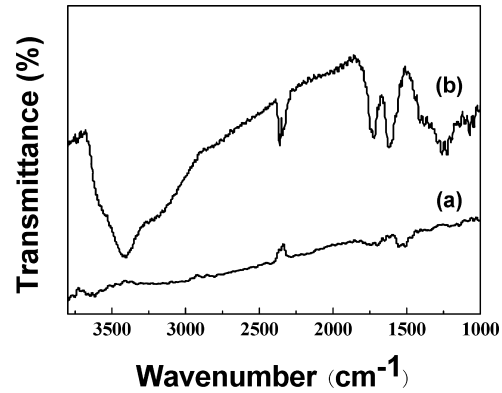

Figure 4. FTIR spectra of (a) pristine CNTs and (b) CNT−COOH.

Although the CNTs have extraordinary properties, most of their applications are thwarted by the difficult transformation into materials that can be uniformly dispersed and easily manipulated in either organic solvents or water.[39−42] Common strategies to overcome this problem are the noncovalent or covalent surface modification to eliminate the highly hydrophobic character of CNTs caused by strong intertubular van der Waals forces.[36,37] In the present study, nitric acid oxidation followed by treating with sodium hydroxide was applied for functionalization of p-CNTs. Successful formation of COOH groups on the side walls of the p-CNTs has been confirmed from bulk measurements including FTIR spectroscopy and TEM observations.[43]

FTIR spectra of the pristine CNTs and the acid-treated CNTs (CNT−COOH) are shown in Figure 4. It can be seen that the FTIR spectrum of the CNT−COOH (Figure 4b) shows two absorption peaks with very strong intensity located at 3448 and 1723 cm^{-1}, corresponding to OH and COOH stretching, respectively. In contrast, these peaks do not appear in the spectrum of pristine CNT (Figure 4a), indicating that a large amount of carboxylic and hydroxyl groups has been generated on the surface of the CNTs by nitric acid treatment.

Figure 5a shows the pristine CNTs with an average diameter of 10−20 nm. After surface oxidation, the surface of the CNTs became heterogeneous due to attack by the oxidative acid. TEM images clearly showed that the smooth surface of the pristine CNTs (Figure 5a) was changed to a much rougher surface (Figure 5b). The acid-treated CNTs can be seen to have an increase in surface roughness as a function of treatment time. The rough surface of the treated CNTs was attributed to the acidic etching of the CNT surfaces.[36,37,43]

In the present study, we prepared LDH/CNT hybrids as illustrated in Figure 6. Through shaking the as-prepared Co−Al−NO_3 LDH sample with formamide for 48 h, a pink and transparent colloidal suspension (Figure 7a) was yielded. Similarly, the CNT−COONa forms a black solution (Figure 7g), demonstrating that there were "soluble" CNTs in the formamide. The interactions between LDH and CNT were investigated by changing the initial volume ratio of LDH suspension to CNT solution. The sedimentation process of LDH suspension can be easily observed from the color change. When stopping shaking, the top regions of the vials with the initial proportion of LDH nanosheets to the CNTs in the range from 1:1 to 1:3 (Figure 5d−f) became colorless and transparent, indicating that the simultaneous sedimentation process of the positively charged LDHs with the negatively charged CNTs

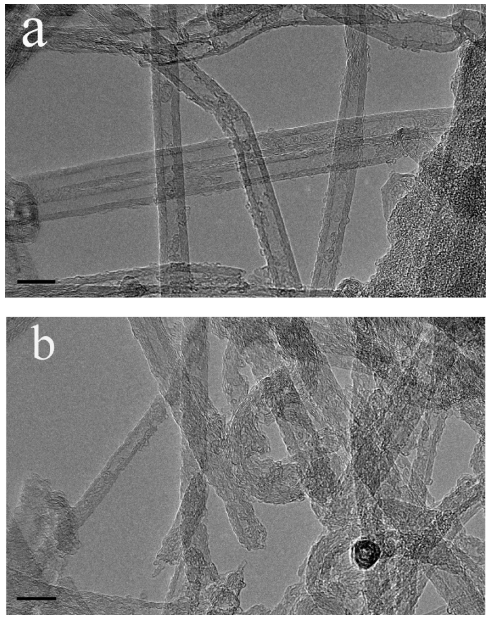

Figure 5. TEM images of (a) pristine CNTs and (b) CNT−COONa. The scale bars indicate 10 nm.

progresses by forming LDH/CNT hybrids via electrostatic force. Therefore, the occurrence of the simultaneous sedimentation of LDH nanosheets with the CNTs at the bottom of the vials implies that there are strong interactions between the LDHs and the CNTs. In contrast, the top regions of the vials with the initial proportion of LDH sheets to the CNTs in the range from 3:1 to 2:1 (Figure 5b to 5c) are dark even after keeping for 72 h, indicating that the CNTs were stabilized by excess LDH and the stable colloidal suspension of LDHs maintained when incorporating a small amount of the CNTs.

Zeta potential is often used as an index of the magnitude of electrostatic interaction between colloidal particles, which is thus a measure of the colloidal stability of the solution.[44,45] Table 1 shows the values of zeta potentials of LDH suspension and LDH/CNT mixtures as a function of CNT content. In the cases of high concentrations of LDHs (LDH to CNT = 3:1 to 2:1), the values of the zeta potential of sample b and sample c (see Figure 7) are 32.1 and 28.9 mV, respectively. This indicates that there are not enough CNTs interacting with LDH nanosheets; thus, the LDH colloid can still keep stable. In addition, the dark color solution is attributed to the small amount of CNTs which are absorbed on the stabilized LDHs. When further adding negatively charged CNTs (zeta potential is −41.4 mV) to the LDH suspension, the values of zeta potentials of samples d, e, and f (as shown in Figure 7) obviously decreased and dropped in the range from −15 to 15 mV. Generally speaking, particles with a zeta-potential value less than 15 mV and no more than −15 mV are expected to be unstable from electrostatic considerations. This is further illustrated by the direct visualization as shown in Figure 7 together with the values of zeta potential listed in Table 1.

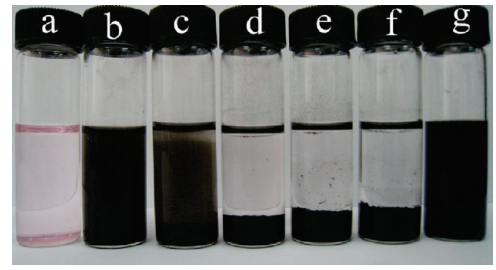

Figure 7. Optical photograph of (a) 1 mg/mL LDH formamide suspension, (b) 3:1, (c) 2:1, (d) 1:1, (e) 1:2, and (f) 1:3 LDH/CNT mixed formamide suspension, and (g) 1 mg/mL CNT formamide solution. (b−f) All are the volume ratios.

TABLE 1: Zeta Potential (ZP) of the LDH (L), CNT (C) Formamide Suspension and the Top Suspension of Mixtures with Different Ratios

sample	L	L:C (3:1)	L:C (2:1)	L:C (1:1)	L:C (1:2)	L:C (1:3)	C
ZP (mV)	36.7	32.1	28.9	11.1	−4.72	−8.82	−41.4

Although anionic NO_3^- balanced the charge of the LDH nanosheets in the suspension, the surface-adsorbed NO_3^- thermally vibrates and temporarily leaves the Stern layer. There are always some anions statistically in the diffusion layer, and thus, the LDH nanoparticles associated with the Stern layer are positively charged. Therefore, the positive zeta potential of LDH particles is in principle attributed to the structural positive charge and the electric double layer on the LDH surface.[46] As known, carboxylic acid groups (COONa) on the surface of the CNTs exist as carboxylate anions (COO^-) in formamide, thus yielding negatively charged CNT. In fact, it is well established that negatively charged nanoparticles or clusters attached to the surfaces of positively charged particles can impart colloidal stability under the dominance of charge attractions. When the initial proportion of the LDH nanosheets to the CNTs was 3:1, a single LDH sheet can interact with a few CNTs in liquid, thus resulting in formation of stable CNT-absorbed LDH sheets, that is, LDH/CNT hybrids for abbreviation here. When increasing the CNT concentration, a single LDH sheet prefers to adsorb excessive CNTs on their surface. Then, the double electric layers of the LDHs will be destroyed, thus leading to severe precipita-

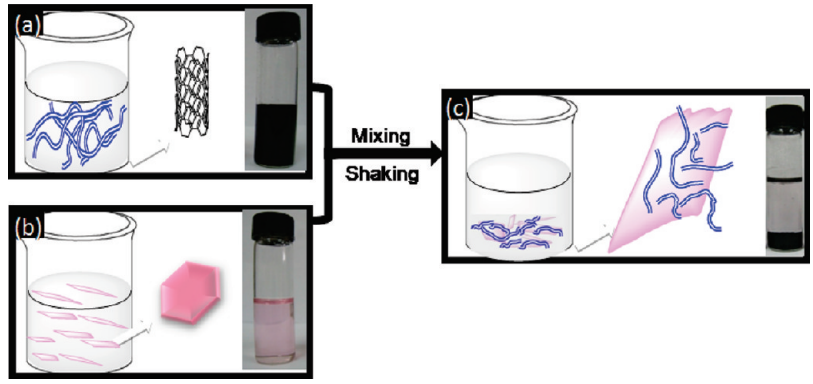

Figure 6. Schematic description of assembling exfoliated LDH/CNT hybrids: (a) CNT formamide suspension, (b) LDH formamide suspension, and (c) mixture of CNT and LDH suspensions.

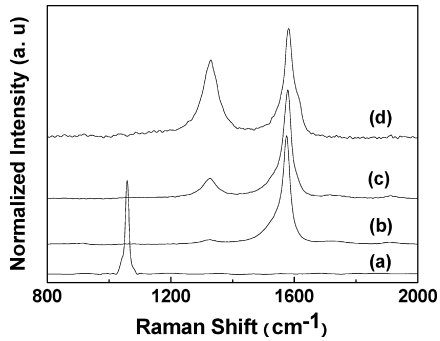

Figure 8. Raman spectra of (a) Co−Al−NO_3 LDH, (b) pristine CNTs, (c) CNT−COONa, and (d) LDH/CNT hybrids.

tion of CNT-coated exfoliated LDH hybrids. Even upon sonicating these sediments for several minutes, the precipitations composed of the exfoliated LDH/CNT hybrids cannot be dispersed or separated and remain at the bottom of the vials.

The interactions of LDH nanosheets with the CNTs were also investigated by Raman spectroscopy, as shown in Figure 8. Co−Al−NO_3 LDHs possess a strong peak at 1059 cm^{-1} (Figure 8a), which is assigned to the symmetry vibration peak of NO_3^-. For the CNTs (Figure 8b), there are always two peaks which are known as the D band and G band. The disordered peak, also known as the D band, can be found in the 1300−1400 cm^{-1} region. This peak is associated with the vibration of carbon atoms with dangling bonds in the plane termination of disordered graphite or glassy carbon. The strength of this peak is related to the amount of disordered graphite and the degree of conjugation disruption in the graphene sheets. The band in the 1500−1600 cm^{-1} region is the G band resulting from the tangential C−C stretching vibrations both longitudinally and transversally on the nanotube axis.[47,48] As can be seen in Figure 8b and 8c, the D/G-band intensity ratio increases after nitric acid treatment, implying that the CNTs with more defects are produced during the oxidation process. This is consistent with the FTIR results in Figure 4 and the TEM images in Figure 5. When the CNTs are interacted with the LDH sheets for the LDH/CNT hybrids sample, not only was the spectral position of the D band and G band shifted but also their spectral intensities were greatly changed (Figure 8d). The Raman spectrum of CNT−COONa (Figure 8c) shows the D band (defects/disorder-induced mode) at 1323 cm^{-1} and G band (in-plane stretching tangential mode) at 1573 cm^{-1}, with a D to G band intensity ratio (I_D/I_G) of 0.18. For the LDH/CNT hybrids, the intensity ratio the D/G band increases to 0.71 with a slight red shift of 3 cm^{-1} at the D band and G band. The strong interaction between positive LDH sheets and negative CNTs increases the energy necessary for vibrations to occur, which is reflected in the higher frequency of Raman peaks. The increase of the D/G band intensity ratio also might be attributed to strong interaction between the LDH sheets with local defects and the CNTs. In addition, the disappearance of the NO_3^- band at 1059 cm^{-1} indicated that the negative CNTs replaced the NO_3^- anion to keep the charge balance of the LDHs.

The microstructures of LDH/CNT hybrids were observed by TEM. Figure 9a shows two-dimensional ultrathin LDH sheets with a lateral dimension of about 1 μm. The nanosheets were morphologically irregular and dimensionally diminished in comparison with the original LDH crystallites (Figure 1), indicating breakage or fracture of the LDH sheets during the delamination and assembling process. At higher magnification (Figure 9b), it can be seen that the surface of the LDH layers adsorbs a lot of CNTs. The tight connection between the CNTs

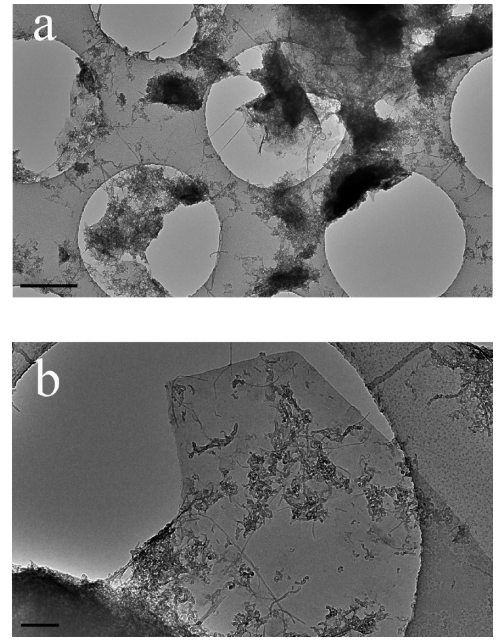

Figure 9. TEM images of (a) low magnification of LDH/CNT hybrids and (b) high magnification of LDH/CNT hybrids. The scale bars in images a and b correspond to 1 μm and 200 nm, respectively.

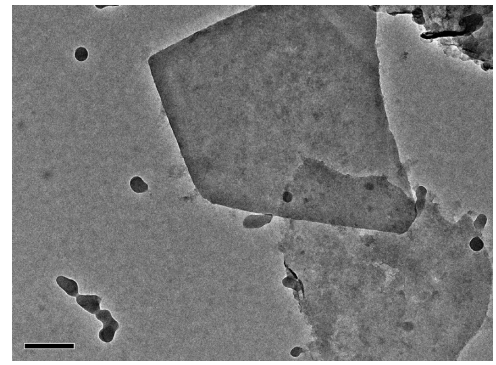

Figure 10. TEM images of exfoliated Co−Al−NO_3 LDH. The scale bar indicates 200 nm.

and the LDH sheets can be obviously observed, and the CNTs were randomly distributed on the surface of LDHs. These results further imply the strong interaction between the CNTs and the LDH sheets. In contrast, Figure 10 shows that the exfoliated LDH nanosheets in formamide have a smooth surface.

In addition, X-ray diffraction was used to study the structures of the exfoliated Co−Al−NO_3 LDH, CNT−COONa, and LDH/CNT hybrid samples, as shown in Figure 11. To explore the exfoliated LDH sample, the suspension was centrifuged for 20 min at a speed of 30 000 rpm to separate a gel-like aggregate from formamide (solvent). The XRD data for the gel-like LDH sample exhibit a pronounced halo in the range of $2\theta = 20-30°$, as depicted in Figure 11a, which can be ascribed to the scattering of liquid formamide. This suggests that the host sheets of LDHs are almost completely swollen and not in a parallel style to induce the interference of the X-rays, implying a successful exfoliation. Figure 11b shows a peak at $2\theta = 26°$ corresponding to the diffraction of layered graphene structure of carbon nanotubes. One of the most striking features for the dry LDH/CNT hybrid sample (Figure 11c) is the absence of the sharp basal peaks, which is in contrast to the XRD pattern of powdery LDH sample (Figure 2). This suggests that the host sheets of LDH are almost completely exfoliated after introducing CNTs

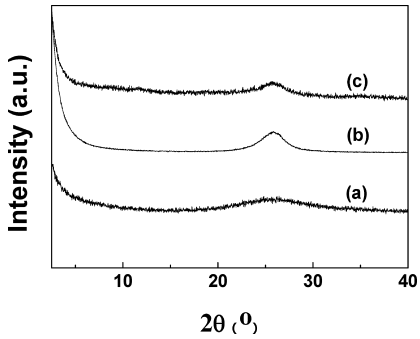

Figure 11. XRD patterns of (a) exfoliated Co−Al−NO_3 LDH, (b) CNT−COONa, and (c) LDH/CNT hybrids.

into the interlayer of LDH. The peak at $2\theta = 26°$ was attributed to diffraction of carbon nanotubes in the hybrids.

Here, we propose a coassembly mechanism based on the above results. First, a certain volume of formamide replaces the water molecules and produces a highly swollen phase and the colloid of highly swollen phase is stable in formamide. Second, when the CNTs are introduced into the colloid, strong electrostatic interaction between the LDH nanosheets and the CNTs may take place, that is, the exfoliated LDH nanosheets with positive charges could adsorb the negatively charged CNTs on their surfaces with the assistance of mechanical shaking. With the increase of the CNT concentration, the stable colloidal state will be destroyed and the LDH nanosheets coated by the CNTs will be precipitated in formamide. Substitution of the CNTs for NO_3^- prevents the LDH nanosheets from restacking into a layered structure of Co−Al−NO_3 LDH when washing with copious amounts of water.

Figure 12a and 12b shows the TEM images of the thin sections of PA6/CNT (1.0 wt %) and PA6/(LDH/CNT) hybrid (2.0 wt %) nanocomposites prepared by in situ polymerization, respectively. For the nanocomposite containing 1 wt % CNTs (Figure 12a), individual CNTs are randomly dispersed within the matrix, as indicated by the red arrows, and no aggregation is observed. The variations in contrast and diameter of the CNTs are mainly due to the difference in electron scattering from different depth regions of the section. The TEM image (Figure 12b) shows that both the exfoliated LDH sheets and the CNTs are dispersed uniformly in PA6 matrix, as indicated by the white arrows and red arrows, respectively. The strong interaction between the LDH nanosheets and the CNTs prevents formation of agglomerates of the LDHs and the CNTs when containing 2 wt % hybrids.

The mechanical properties of neat PA6 and its nanocomposites from tensile testing (Figure 13) are summarized in Table 2. Note that it is difficult to be exfoliated for the Co−Al−NO_3 LDHs in the matrix without surface modification by dodecyl sulfate. Therefore, the mechanical property data of the binary PA6/LDH nanocomposites reported in our previous work[38] were used here for comparison. With incorporation of 2 wt % LDH/CNT hybrids, compared to neat PA6, the tensile modulus of the nanocomposites is increased by 210% from 1.0 to 3.1 GPa and the tensile strength is increased by 35% from 55.0 to 74.3 MPa. The increase of tensile modulus and tensile strength of the binary nanocomposites is saturated at 1.0 wt % LDHs for the PA6/LDH system and 1.0 wt % CNTs for the PA6/CNT system, which may be caused by aggregation of the nanofillers at higher contents. Both the tensile strength and the modulus of ternary PA6/hybrid composites are much higher than the corresponding binary PA6/LDH (2.0 GPa and 62.1 MPa) or PA6/CNT (2.5 GPa and 63.9 MPa) nanocomposites. The

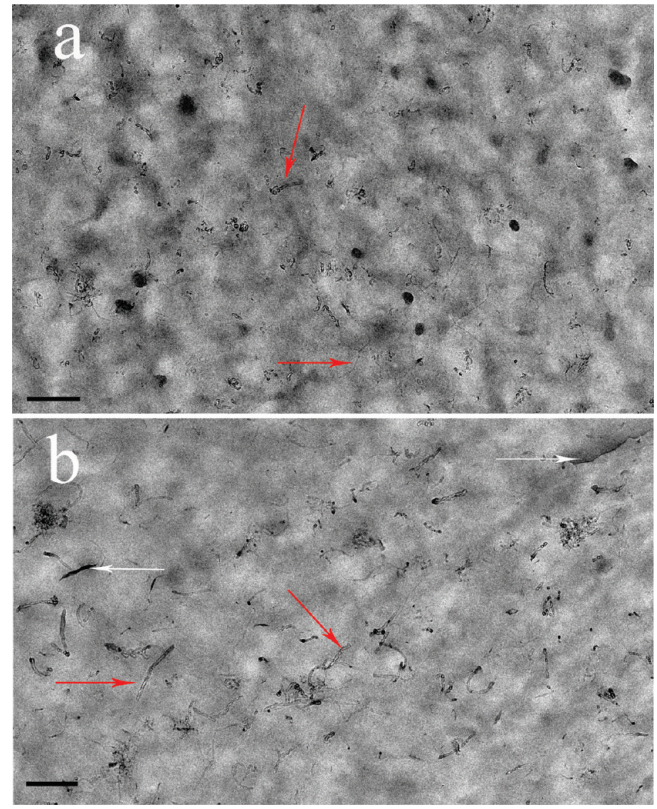

Figure 12. TEM images of PA6 nanocomposites: (a) PA6/CNT (1.0 wt %) and (b) PA6/(LDH/CNT) hybrid (2.0 wt %) nanocomposite. The scale bars indicate 200 nm.

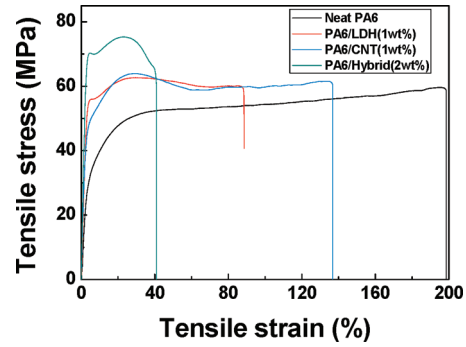

Figure 13. Typical stress−strain curves of neat PA6 and its nanocomposites.

TABLE 2: Summary of Mechanical Properties of Neat PA6 and Its Nanocomposites

sample	tensile modulus (GPa)	tensile strength (MPa)	elongation at break (%)
Neant PA6	1.0 ± 0.1	55.0 ± 0.3	220.0 ± 33.6
PA6/LDH(1.0 wt %)	2.0 ± 0.1	62.1 ± 0.2	74.8 ± 12.5
PA6/CNT(1.0 wt %)	2.5 ± 0.1	63.9 ± 0.1	102.3 ± 22.5
PA6/Hybrid(2.0 wt %)	3.1 ± 0.1	74.3 ± 0.5	41.5 ± 5.6

significant reinforcement by using the LDH/CNT hybrids is obviously related to the synergistic effect of the CNTs and the LDH nanoplatelets for their homogeneous dispersion and strong interaction with the polymer matrix, which favor efficient stress transfer from the matrix to the nanofillers. However, the improvement of mechanical properties of PA6 nanocomposites is accompanied with an obvious decrease of elongation at break, from 220% for neat PA6 to 41.5% for the ternary PA6/(LDH/CNT) systems. The decrease of toughness is probably attributed to the mobility confinement of PA6 chains, resulting from the

restriction effect due to the presence of the nanofillers.[49] These results were in good agreement with our previous report on the 3D nanostructured fillers by growing the carbon nanotubes onto the clay platelets.[29]

4. Conclusions

In summary, highly crystalline and monodispersive Co−Al−CO_3 LDH samples were prepared by precipitation through urea hydrolysis under hydrothermal condition. LDHs were highly swollen in formamide after decarbonation and anion exchange to Co−Al−NO_3 LDHs. The negatively charged and soluble CNTs (CNT−COONa) were prepared by nitric acid oxidation followed by treating with sodium hydroxide. When the CNTs are introduced into the colloidal suspension of Co−Al−NO_3 LDHs, stronger electrostatic interaction between the LDHs and the CNTs may take place. The exfoliated LDH nanosheets with positive charges could adsorb negative CNTs on their platelet surfaces with the assistance of mechanical shaking. This is a simple method for preparing exfoliated LDH nanosheet/CNT hybrids with all metal kinds of LDHs. The LDH/CNT hybrids with unique 3D nanostructure are novel nanofillers which combine 2D LDH platelets and 1D carbon nanotubes together. Furthermore, the synergic effect of the CNTs and the LDH platelets in the hybrids can find promising applications for fabrication of high-performance and multifunctionality polymer nanocomposites due to fine dispersion of the functional nanofillers and strong interactions with the matrix.

Acknowledgment. The authors are grateful for financial support from the National Natural Science Foundation of China (20774019; 50873027), Fudan Innovation Funds for Excellent Graduate, "Shu Guang" project (09SG02) supported by the Shanghai Municipal Education Commission and Shanghai Education Development Foundation, and the Open Research Fund of State Key Laboratory of Polymer Physics and Chemistry, Changchun Institute of Applied Chemistry, Chinese Academy of Sciences.

References and Notes

(1) Hetterley, R. D.; Mackey, R.; Jones, J. T. A.; Khimyak, Y. Z.; Fogg, A. M.; Kozhevnikov, I. V. *J. Catal.* **2008**, *258*, 250.
(2) Oliver, S. R. J. *Chem. Soc. Rev.* **2009**, *38*, 1868.
(3) Zhao, Y. F.; Wei, M.; Lu, J.; Wang, Z. L.; Duan, X. *ACS Nano* **2009**, *3*, 4009.
(4) Wang, Y. F.; Gao, H. Z. *J. Colloid Interface Sci.* **2006**, *301*, 19.
(5) Olfs, H. W.; Torres-Dorante, L. O.; Eckelt, R.; Kosslick, H. *Appl. Clay Sci.* **2009**, *43*, 459.
(6) Reinholdt, M. X.; Babu, P. K.; Kirkpatrick, R. J. *J. Phys. Chem. C* **2009**, *113*, 3378.
(7) Hussein, M. Z. bin; Zainal, Z.; Yahaya, A. H.; Foo, D. W. V. *J. Controlled Release* **2002**, *82*, 417.
(8) Tammaro, L.; Costantino, U.; Nocchetti, M.; Vittoria, V. *Appl. Clay Sci.* **2009**, *43*, 350.
(9) Gunawan, P.; Xu, R. *J. Phys. Chem. C* **2009**, *113*, 17206.
(10) Delahaye, E.; Eyele-Mezui, S.; Bardeau, J. F.; Leuvrey, C.; Mager, L.; Rabu, P.; Rogez, G. *J. Mater. Chem.* **2009**, *19*, 6106.
(11) Han, J. B.; Yan, D. P.; Shi, W. Y.; Ma, J.; Yan, H.; Wei, M.; Evans, D. C.; Duan, X. *J. Phys. Chem. B* **2010**, *114*, 5678.
(12) Ye, L.; Ding, P.; Zhang, M.; Qu, B. J. *J. Appl. Polym. Sci.* **2008**, *107*, 3694.
(13) Pereira, C. M. C.; Herrero, M.; Labajos, F. M.; Marques, A. T.; Rives, V. *Polym. Degrad. Stab.* **2009**, *94*, 939.
(14) Costa, F. R.; Wagenknecht, U.; Heinrich, G. *Polym. Degrad. Stab.* **2007**, *92*, 1813.
(15) Du, L. C.; Qu, B. J. *J. Mater. Chem.* **2006**, *16*, 1549.
(16) Illaik, A.; Taviot-Gueho, C.; Lavis, J.; Cornmereuc, S.; Verney, V.; Leroux, F. *Chem. Mater.* **2008**, *20*, 4854.
(17) O'Leary, S.; O'Hare, D.; Seeley, G. *Chem. Commun.* **2002**, *14*, 1506.
(18) Hibino, T.; Jones, W. *J. Mater. Chem.* **2001**, *11*, 1321.
(19) Li, L.; Ma, R. Z.; Ebina, Y.; Iyi, N.; Sasaki, T. *Chem. Mater.* **2005**, *17*, 4386.
(20) Liu, Z. P.; Ma, R. Z.; Osada, M.; Iyi, N.; Ebina, Y.; Takada, K.; Sasaki, T. *J. Am. Chem. Soc.* **2006**, *128*, 4872.
(21) Li, L.; Ma, R. Z.; Ebina, Y.; Fukuda, K.; Takada, K.; Sasaki, T. *J. Am. Chem. Soc.* **2007**, *129*, 8000.
(22) Iijima, S. *Nature* **1991**, *354*, 56.
(23) Baughman, R. H.; Zakhidov, A. A.; De Heer, W. A. *Science* **2002**, *297*, 787.
(24) Kovtyukhova, N. I.; Mallouk, T. E.; Pan, L.; Dickey, E. C. *J. Am. Chem. Soc.* **2003**, *125*, 9761.
(25) Dai, H. *Acc. Chem. Res.* **2002**, *35*, 1035.
(26) Costache, M. C.; Heidecker, M. J.; Manias, E.; Camino, G.; Frache, A.; Beyer, G.; Gupta, R. K.; Wilkie, C. A. *Polymer* **2007**, *48*, 6532.
(27) Su, L. H.; Zhang, X. G. *J. Power Sources* **2007**, *172*, 999.
(28) Georgakilas, V.; Gournis, D.; Karakassides, M. A.; Bakandritsos, A.; Petridis, D. *Carbon* **2004**, *42*, 865.
(29) Zhang, W. D.; Phang, I. Y.; Liu, T. X. *Adv. Mater.* **2006**, *18*, 73.
(30) Sun, D.; Chu, C. C.; Sue, H. J. *Chem. Mater.* **2010**, *22*, 3773.
(31) Zhao, M. Q.; Zhang, Q.; Jia, X. L.; Huang, J. Q.; Zhang, Y. H.; Wei, F. *Adv. Funct. Mater.* **2010**, *20*, 677.
(32) Cao, Y.; Zhao, Y.; Li, Q. X.; Jiao, Q. Z. *J. Chem. Sci.* **2009**, *121*, 225.
(33) Shaijumon, M. M.; Bejoy, N.; Ramaprabhu, S. *Appl. Surf. Sci.* **2005**, *242*, 192.
(34) Xiang, X.; Zhang, L.; Hima, H. I.; Li, F.; Evans, D. G. *Appl. Clay Sci.* **2009**, *42*, 405.
(35) Huang, S.; Cen, X.; Peng, H. D.; Guo, S. Z.; Wang, W. Z.; Liu, T. X. *J. Phys. Chem. B* **2009**, *113*, 15225.
(36) Salzmann, C. G.; Llewellyn, S. A.; Tobias, G.; Ward, M. A. H.; Huh, Y.; Green, M. L. H. *Adv. Mater.* **2007**, *19*, 883.
(37) Yu, H.; Jin, Y. G.; Peng, F.; Wang, H. J.; Yang, J. *J. Phys. Chem. C* **2008**, *112*, 6758.
(38) Peng, H. D.; Tjiu, W. C.; Shen, L.; Huang, S.; He, C. B.; Liu, T. X. *Compos. Sci. Technol.* **2009**, *69*, 991.
(39) O'Connell, M. J.; Bachilo, S. M.; Huffman, C. B.; Moore, V. C.; Strano, M. S.; Haroz, E. H.; Rialon, K. L.; Boul, P. J.; Noon, W. H.; Kittrell, C.; Ma, J. P.; Hauge, R. H.; Weisman, R. B.; Smalley, R. E. *Science* **2002**, *297*, 593.
(40) Richard, C.; Balavoine, F.; Schultz, P.; Ebbesen, T. W.; Mioskowski, C. *Science* **2003**, *300*, 775.
(41) Dieckmannm, G. R.; Dalton, A. B.; Johnson, P. A.; Razal, J.; Chen, J.; Giordano, G. M.; Munoz, E.; Musselman, I. H.; Baughman, R. H.; Draper, R. K. *J. Am. Chem. Soc.* **2003**, *125*, 1770.
(42) Zheng, M.; Jagota, A.; Semke, E. D.; Diner, B. A.; McLean, R. S.; Lustig, S. R.; Richardson, R. E.; Tassi, N. G. *Nat. Mater.* **2003**, *2*, 338.
(43) Xing, Y. C.; Li, L.; Chusuei, C. C.; Hull, R. V. *Langmuir* **2005**, *21*, 4185.
(44) White, B.; Banerjee, S.; O'Brien, S.; Turro, N. J.; Herman, I. P. *J. Phys. Chem. C* **2007**, *111*, 13684.
(45) Wang, Z.; Meng, X. Y.; Li, J. Z.; Du, X. H.; Li, S. Y.; Jiang, Z. W.; Tang, T. *J. Phys. Chem. C* **2009**, *113*, 8058.
(46) Xu, Z. P.; Jin, Y. G.; Liu, S. M.; Hao, Z. P.; Lu, G. Q. *J. Colloid Interface Sci.* **2008**, *326*, 522.
(47) Irle, S.; Mews, A.; Morokuma, K. *J. Phys. Chem. A* **2002**, *106*, 11973.
(48) Vix-Guterl, C.; Couzi, M.; Dentzer, J.; Trinquecoste, M.; Delhaes, P. *J. Phys. Chem. B* **2004**, *108*, 19361.
(49) Leroux, F.; Illaik, A.; Stimpfling, T.; Troutier-Thuilliez, A. L.; Fleutot, S.; Martinez, H.; Cellier, J.; Verney, V. *J. Mater. Chem.* **2010**, *20*, 9484.

JP1087256